Tomoyuki Suzuki[1], Masashi Kamogawa[1], Hironobu Fujiwara[2], and Syugo Hayashi[3]

[1] University of Shizuoka, Shizuoka, 4200839, Shizuoka, Japan.

[2] Waseda University, 1690072, Tokyo, Japan.

[3] Meteorological Research Institute, Japan Meteorological Agency, 3050052, Ibraki, Japan.

Corresponding author: Tomoyuki Suzuki (suzuki2020@u-shizuoka-ken.ac.jp)

Key Points:

- Six sprites were observed on 22 July 2013 from Mt. Fuji and five occurred over stratiform region and one occurred over convective region.
- Time to the peak in strong precipitation rate versus total precipitation with the first sprite and that with the last one were different.
- The time differences until peaks may indicate that the charging mechanisms are different between the stratiform and convective regions.

Abstract

Six sprites were observed on 22 July 2013 from Mt. Fuji (3776 m above sea level), Japan. Five of six sprite-producing positive cloud-to-ground strikes (SP +CGs) occurred in the stratiform region, while one SP +CG occurred in the convective region. Time sequences and horizontal evolution of precipitation between these regions with sprites were analyzed. Prior to the first five sprites, the areal amount of strong precipitation (8 mm/h) increased considerably. However, such an increase did not occur with the sixth sprite. The sprites occurred at the local peaks in strong precipitation rate with respect to total precipitation. The rise time to the first peak with the first sprite was 80 minutes, while the rise time to the last peak with the sixth sprite was 30 minutes. These temporal differences until peaks may indicate that the charging mechanisms due to precipitation are different between the stratiform and convective regions.

Plain Language Summary

Upper atmospheric transient luminous events (TLEs) such as sprites are usually observed from the ground using high-sensitivity cameras. The view from a high mountain above low clouds provides a better chance of detecting TLEs than that from the ground. The high-mountain observations during the summer of 2013 were made at the summit of Mt. Fuji (3776 m above sea level), Japan. On 22 July 2013, we succeeded in detecting six sprites. Five of the six sprite-producing positive cloud-to-ground strikes (SP +CGs) occurred in the stratiform region, while one SP +CG occurred in the convective region. To investigate the difference in precipitation between these regions, time sequences and horizontal evolution of precipitation were analyzed in the north-central area of Japan. In all cases, sprites occurred at the local peaks of the percentage of strong precipitation with respect to total precipitation. The period of increase

before the first peak with the first sprite above the stratiform region was 80 minutes, while the period of increase before the last peak with the last sprite above the convective region was 30 minutes. These temporal differences may indicate that the charging mechanisms due to precipitation differ between the stratiform and convective regions.

Keywords: Sprite, precipitation rate, Mesoscale Convective System, charging in stratiform and convective region, Transient luminous events (TLEs), lightning

1 Introduction

Sprites, which are mesospheric transient luminous events (TLEs), occur above large thunderstorm systems, such as mesoscale convective systems (MCSs), and coincide with large positive cloud-to-ground lightning strokes (+CGs) (Sentman and Wescott, 1996). The first report of TLEs was sprites and was observed in North America in 1989 (Franz et al., 1990). Many investigations and observation campaigns for TLEs have been conducted since the 1990s, and numerous TLEs have been detected all over the world (e.g., in summer: Frantz et al., 1990; Neubert et al., 2001; Pinto et al., 2004; Su et al., 2002; Suzuki et al., 2012; Williams et al., 2010. In winter: Adachi et al., 2005; Fukunishi et al., 1999; Ganot et al., 2007; Hayakawa et al., 2004; Soula et al., 2010; Suzuki et al., 2006; Takahashi et al., 2003).

It is well known that CGs occur very actively in the summer in Japan. There is a high CG flash density of more than 1.5×10^{-3} flashes km^{-2} day^{-1} in inland Japan during summer and a maximum of 12.0×10^{-3} flashes km^{-2} day^{-1} on the Kanto Plain (Ishii et al., 2014). This indicates that a large number of summer thunderstorms with active CGs are produced in inland Japan. Many clusters of blue jets and blue starters, which are also TLEs, have appeared above the Kanto Plain (Suzuki et al., 2012). Therefore, it is expected that other types of TLEs, such as sprites, halos, elves, and jet-like events, are produced over inland Japan.

TLEs are usually observed from ground-based stations, and the success of TLE observations largely depends on the cloud (weather) conditions between the TLEs and the stations—clouds prevent observations. To work around these issues, TLE observations from high mountain summits offer higher vantage points, greater atmospheric transparency, and better cloud conditions. TLE observations from mountain summits have been reported by Neubert et al. (2001; 2005) and van der Velde et al. (2006) as part of the EuroSprite campaign. They collected many sprite images with a light-sensitive camera system mounted at the Observatory Midi-Pyrénées on Pic du Midi in the French Pyrenees at an altitude of 2877 m above sea level. They demonstrated the merits of observing TLEs from high mountains.

To detect TLEs above the Kanto Plain, we conducted a campaign from the weather station at the summit of Mt. Fuji, the highest mountain in Japan (altitude 3776 m), from 18 July to 11 August 2013. The summit of Mt. Fuji provides a 360° view and high vantage point. These may permit clear images of TLEs

and details of their morphology to be observed. In addition, TLEs, their related lightning, and their parent thunderstorms can be detected simultaneously. We installed a high-sensitivity monochrome video camera at the Mt. Fuji Weather Station, focused toward the Kanto Plain (inland), and the camera operated during night time (Figure 1a). We succeeded in capturing six sprite video images on 22 July 2013. Sample images of sprites are shown in Figure 1b and c. We selected the sprite parent thunderstorm using radar echo data and directions of sprite events. Consequently, it was found that five of the six sprites were produced by +CGs in the stratiform region, and one was produced by +CG in the convective region in MCS. The characteristics of sprite-producing +CGs in the convective and stratiform regions reflect the charging mechanisms due to precipitation particles inside each region. In this study, we show the temporal and spatial evolution of the sprite parent thunderstorm system from the time sequences of the total amount of strong and weak precipitation and spatially integrated precipitation.

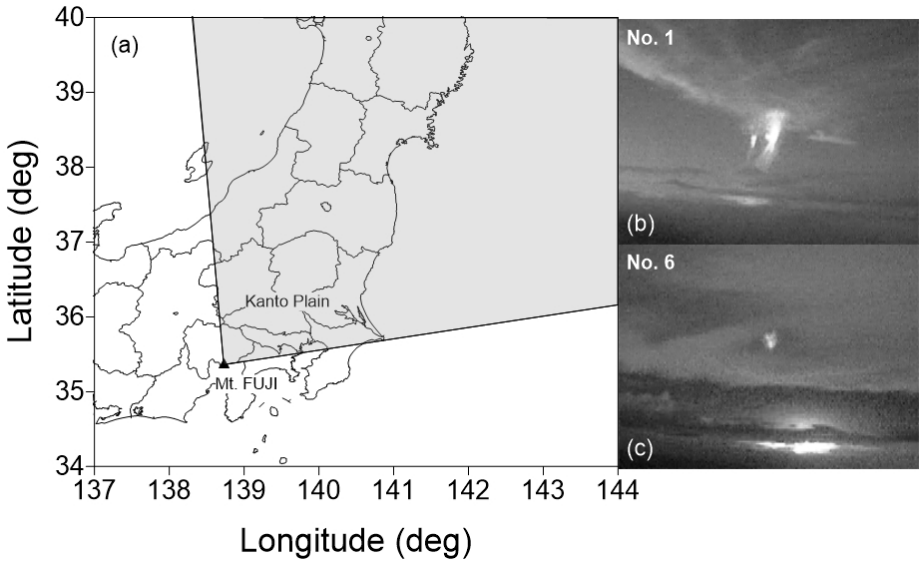

Figure 1. (a) Configuration of the TLE observations for the 2013 Mt. Fuji campaign. The shadow denotes the detectable area for TLEs from the summit of Mt. Fuji (black triangle:) using a monochrome camera. (b) First and (c) last (sixth) of six sprite images observed from the summit of Mt. Fuji on 22 July 2013.

2 Observations and Data

The configuration used for the TLE observations and analysis area are shown in Figure 1. A light-sensitive monochrome charge coupled device (CCD) video camera was mounted at the Mt. Fuji Weather Station. The camera specifications were as follows: The monochrome camera (WAT910HX; Watec Co., Ltd.) was equipped with a 4-mm lens (CBC Co., Ltd. TG0412FCS-3, 1/3" f4.0 mm F1.2;

field of view: 83.49 (H), 64.56 (V)). The WAT910HX is a dark-field CCD camera with ultrahigh light sensitivity, containing a 1/2-inch monochrome imager (minimum illumination: 0.000005 lx at F1.4; effective pixels: 0.38 M). Timestamps synchronized with a global positioning system (GPS) were superimposed onto the video field with a GPS time imposer. The duration of one video field de-interlaced from one video frame (1/30 s) was 16.7 ms (1/60 s). Sprites could occur somewhere between the beginning and end of the field. When a sprite is captured in one field, 16.7 ms is the maximum uncertainty; the uncertainty increases when the sprite is captured in multiple fields. The video signal from the CCD camera was separated via an antenna splitter. Two separated video lines were connected to a hard-disk video recorder and PC via a video capture board (Grass Valley K.K. ADVC-5). The camera, protected a camera housing, was fixed outside the Mt. Fuji Weather Station and was focused toward the Kanto Plain (aimed to the north). The monochrome CCD camera systems were operated from 0900 Universal Time Coordinated (UTC) to 2000 UTC. Automated event detection software (UFO capture V2; triggering level for the unmasked region: 30) stored the video images beginning 5 s before and ending 5 s after detection of an event. In addition, to prevent missing event detection, the hard-disk recorders continuously captured CCD images during this period.

To investigate the properties of the CGs, we used very high frequency (VHF)/low frequency (LF) lightning mapping data detected by the Lightning Detection Network (LIDEN), operated by the Japan Meteorological Agency (JMA). The LIDEN is a hybrid system comprising a VHF array and an LF detector to collect interferometric and time-of-arrival (TOA) measurements based on VHF and LF signals, respectively. This system is in use at 30 sites in Japan (Ishii et al., 2014). Several properties of the CGs, such as location, time, peak current amplitude, current polarity, and lightning type were analyzed. The locations of the VHF radiation sources generated within clouds was triangulated by at least two VHF sites. The 2D locations of the CGs were detected by several LF detectors and estimated from TOA measurements.

The parent thunderstorm was identified by composite radar echo maps generated by twenty C-band weather radars operated by JMA, and precipitation was corrected with ground-based precipitation observations. The composite radar echo maps provided information every 10 minutes about the precipitation near the ground at an altitude of 2 km with a resolution of 1 km $\times$ 1 km. Time sequences of areal and horizontal precipitation integrated every two hours were produced from these radar data.

3 Results and Discussion

House (1977) reported time variations in the anvil (stratiform) and convective areas in linear MCSs that were analyzed using C-band radar and meteorological satellite images. He defined the criteria simply as echo intensities of 29 dBZ (3mm/h) between anvil(stratiform) boundary and squall-line (convective) and showed time series of precipitation with respect to both. Rutledge and McGorman (1988) described a correlation between increase of areally integrated

stratiform precipitation and the frequency of positive CG flashes. Time series of precipitation areas and quantities were also mentioned by Soula et al. (2010) and Hayakawa et al. (2004). To extract more detail from the time sequence of the amount of precipitation in the sprite parent thunderstorm system on 22 July 2013, we categorized precipitation rates and areas in the JMA composite radar echo from 0.2 to 1 mm/h; from 1 to 2 mm/h; from 2 to 4 mm/h; from 4 to 8 mm/h; from 8 to 16; from 16 to 32 mm/h; from 32 to 260 mm/h (not shown). As a result, there was an obvious difference for the time sequences of less than 8 mm/h and more than 8 mm/h total precipitation rate and area. The time sequence was simpler than that presented by Soula et al. (2010). We define precipitation rates less than 8 mm/h as weak precipitation and more than 8 mm/h as strong precipitation. The weak precipitation in total had bimodal peaks, while the strong precipitation had a unimodal peak (shown in Figure 2). We focused on the time sequence of strong and weak precipitation and studied the relationship between sprite emission and precipitation.

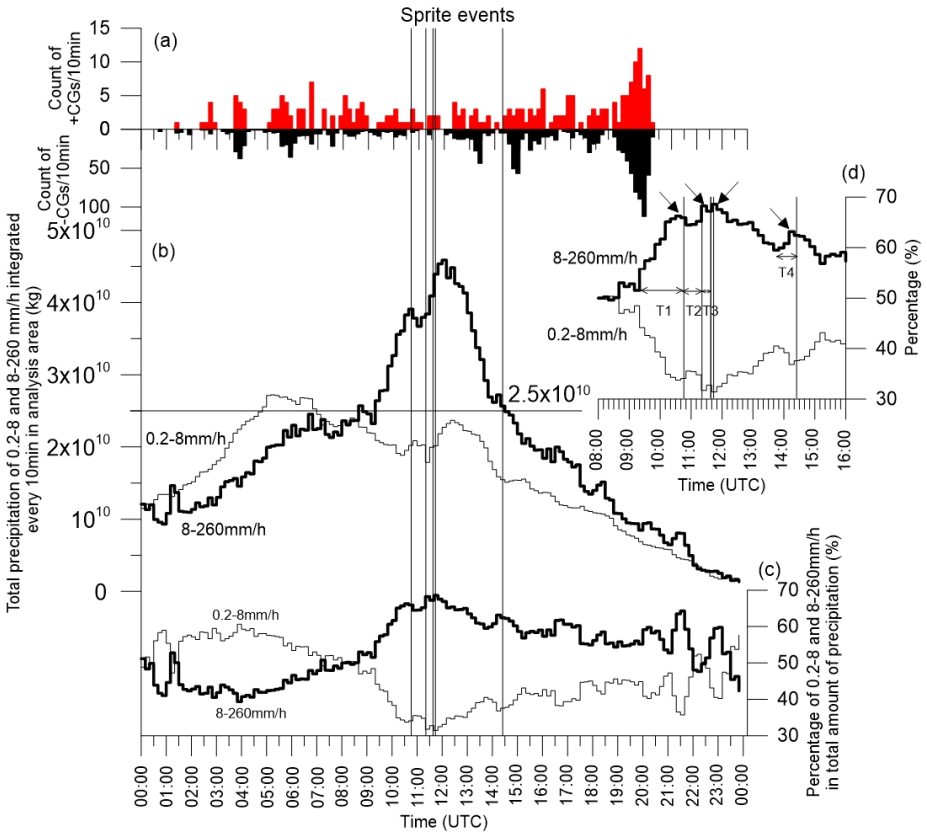

Figure 2. Time sequence of the number of +CG (red) and −CG (black) every 10 min (upper graph:a) and time sequence of the total precipitation integrated every 10 min for 0.2–8 mm/h (thin line graph) and 8–260 mm/h (bold line

graph) derived from the JMA radar echo composite maps during the parent thunderstorm systems (left scale:b). Time sequence of percentage of strong (8–260 mm/h) and weak precipitation (0.2–8 mm/h) versus total precipitation (right scale:c). Vertical solid lines indicate sprite occurrence times. An enlarged graph between 0800 and 1600 UTC of the bottom graph is shown in the middle graph (d). Arrows indicate peaks.

Figure 2a shows the time sequence of ±CG counts in 10-minute increments and sprite events (vertical thin lines). Both positive and negative CG activity was very low before and during five of the sprite emissions. After the fifth sprite, CG activity temporarily increased before decreasing near the time of the last sprite event and increasing again after. This point is the difference in behavior between the CG activity that produced the first five sprites and that which produced the last sprite.

Figure 2b shows the time sequence of integrated precipitation every 10 minutes in the weak (0.2–8 mm/h) and strong (8–260 mm/h) precipitation areas in the analysis region covering 34–40°N and 137–144°E. As mentioned, integrated weak precipitation had a bimodal shape and strong precipitation had a unimodal shape. The maximum precipitation rate was 4.8×10^{10}kg/10 minutes and five sprites were observed 1–1.5 h before the peak of strong precipitation. The last sprite seems to be associated with a temporary small increase in strong precipitation. Sprites were produced when the rate of precipitation surpassed 2.5×10^{10}kg/10 minutes in total. There was a larger areal amount of weak precipitation than strong precipitation before 0800 UTC. After that, the amount of strong precipitation increased considerably in spite of the decrease in weak precipitation. This time sequence may indicate that the characteristics of the precipitation produced within the storm system changed after 0800 UTC. That is, it suggests that total precipitation consisted of a larger area of weak precipitation and a smaller area of strong precipitation until 0800 UTC. Then, both weak and strong precipitation reached a maximum or local peak around 1200 UTC. The strong precipitation peak was two times larger than the two weak precipitation peaks. These seem to suggest that sprite emission is associated with the total amount of strong precipitation. The relationship between them was analyzed using the rate of change of strong precipitation within the total amount of precipitation. This rate shows how rapidly the amount of strong precipitation under the thunderstorm system increased.

Figure 2c shows the time sequence of the rate of change of strong precipitation versus total precipitation. It seems that sprites occurred very close to the local peaks in the rate of change. As we referred to previously, Rutledge and MacGorman (1988) found a correlation between areally integrated stratiform precipitation and the frequency of positive CG flashes. Similarly, at least for our sprites, there seems to be a correlation between the rate of strong precipitation (8 mm/h) contained in the total precipitation and the occurrence of sprite-producing +CGs (and, therefore, sprite emissions).

Figure 2d shows the enlarged graph of Figure 2c between 0800 and 1600 UTC. As

before, the characteristics of strong and weak precipitation changed after 0800 UTC. After the change, the rate of strong precipitation gradually accelerated 1.5–2 hours before the first sprite before decreasing temporarily. Later, the rate increased again, and then the second to fifth sprites occurred close to local peaks in the rate of change. After that, the rate increased suddenly just before the final sprite occurred. Time periods of positive gradients (increasing strong precipitation) in the change rate were 80 minutes (until the first sprite:T1), 30 minutes (second sprite:T2), 10 minutes (third, fourth, and fifth sprites:T3), and 30 minutes (sixth sprite:T4), respectively. The first-fifth sprites were produced in the same storm but the last sprite was produced in the different storm. The differences in the time periods of the positive gradients for the first and the last sprite may suggest a difference in the charging mechanism due to precipitation.

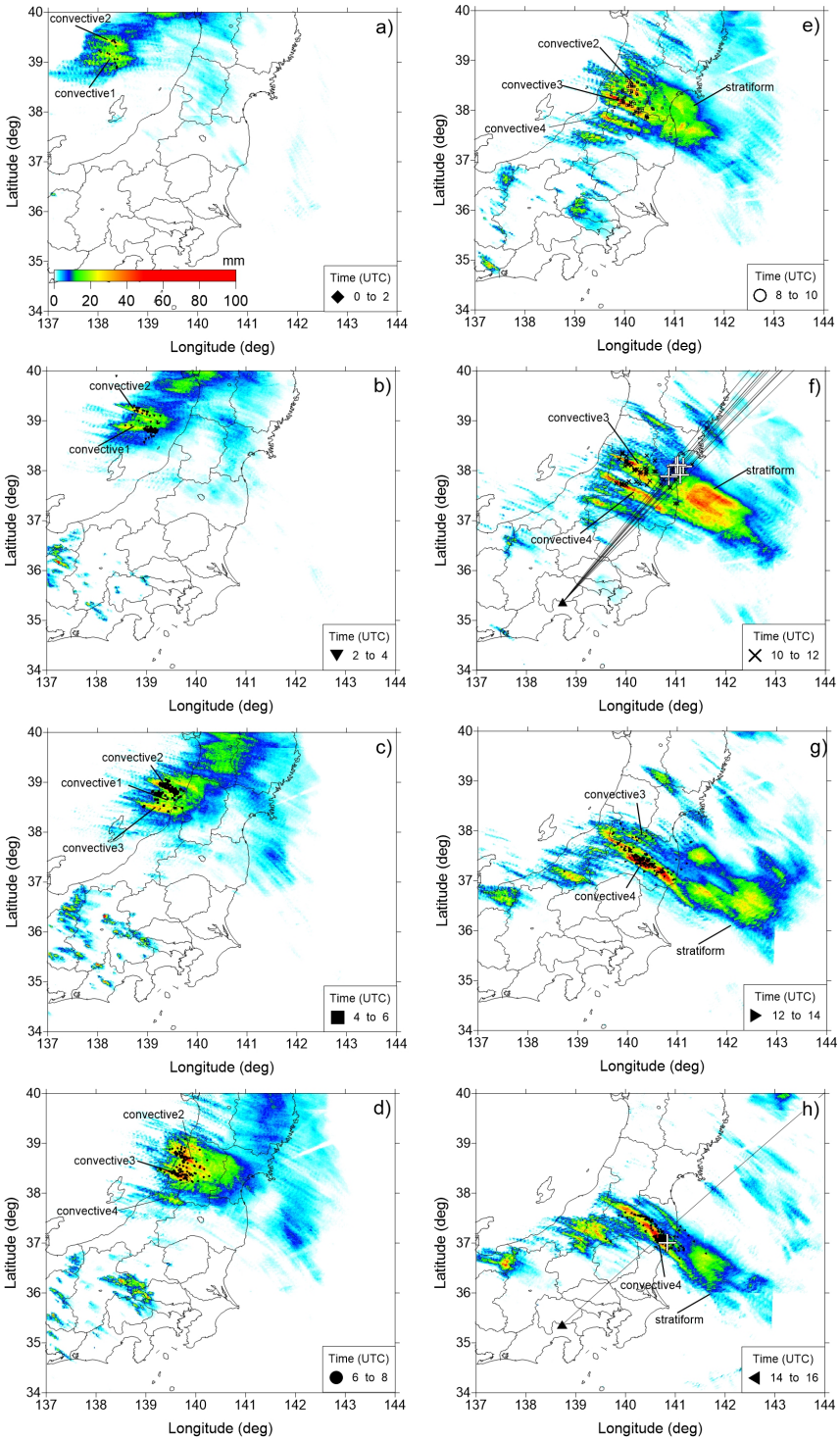
a)
convective2
convective1
mm
0 20 40 60 80 100
Time (UTC)
0 to 2
b)
convective2
convective1
Time (UTC)
2 to 4
c)
convective2
convective1
convective3
Time (UTC)
4 to 6
d)
convective2
convective3
convective4
Time (UTC)
6 to 8
e)
convective2
convective3
convective4
stratiform
Time (UTC)
8 to 10
f)
convective3
convective4
stratiform
Time (UTC)
10 to 12
g)
convective3
convective4
stratiform
Time (UTC)
12 to 14
h)
convective4
stratiform
Time (UTC)
14 to 16
Latitude (deg)
Longitude (deg)

Figure 3. Time series of precipitation integrated in the sprite parent thunderstorm system and locations of CG. Steps in the evolution of the parent thunderstorm system were denoted by total precipitation every two hours integrated. CGs were indicated by various black markers (see the lower right legend in each panel). The large white crosses were sprite-producing +CGs. Convective and stratiform regions are shown with the letters "convective" and "stratiform." The solid lines from Mt. Fuji indicate the azimuthal positions of sprite elements.

Figure 3 shows the CG locations and total precipitation calculated from JMA radar data at an altitude of 2 km and integrated every two hours. The selected area shown in Figure 3 (34–40°N, 137–144°E) is the same as Figure 2 and includes the CGs and total precipitation integrated over the lifetime of the sprite parent thunderstorm system, from its development to dissipation, before and after sprite emission. Solid lines on Figures 3f and 3h indicate the azimuthal locations of sprites from Mt. Fuji (black triangle at the origin of the solid lines).

The thunderstorm system with developing had moved into the analysis area at 0000–0200 UTC (Figure 3a). Two convective lines (convective 1 and convective 2) were located in the thunderstorm system until 0200–0400 UTC (Figure 3b). After 0400 UTC, a third convective line (convective 3) appeared and began to form a stratiform region to the east of the convective 1 and convective 2 lines in the thunderstorm system (figure 3d). Convective 1 dissipated, and a new convective line (convective 4) appeared to the south of convective 3 in the thunderstorm system by 0800 UTC. The stratiform region extended more to the east of these convective lines (Figure 3e). The area in the stratiform region became larger and the intensity of precipitation was much stronger than in the preceding time period. Sprite producing +CGs were located under the azimuth lines of elements of sprite 1–5 (Figure 3f). These +CGs and sprites clustered on the west side of the intense precipitation area in the stratiform region. This may mean that sprites 1–5 were produced by +CGs in the stratiform region and the +CG causative charge was generated there. Precipitation in the stratiform region in this period (1000–1200 UTC) became considerably greater than in the previous period (before 1000 UTC). As illustrated in Figure 2, the amount of strong precipitation between 0900 and 1200 UTC increased considerably. The stratiform region contained two band-like intense precipitation areas (but no convective cells) and was larger than the convective areas (Figure 3f). As you can also see in Figure 3f, the intense precipitation in the stratiform region was the area that contributed most to the strong precipitation peaks (8 mm/h) associated with five sprites in Figure 2. Intense precipitation in the stratiform region during this period would have been associated with the largest total precipitation peak in the strong precipitation time sequence during the same period. The total precipitation area (0.2 mm/h) surpassed 60000 km^2 when the first sprite occurred, and then it peaked at 67000 km^2 at 1210 UTC. Lyons (1996) reported that summer sprite parent MCSs in the central United States have contiguous radar reflectivity areas exceeding 20–25,000 km^2. Further, stratiform regions developing ahead of the convective core and its area with reflectivity larger than 10 dBZ at an altitude of 3000 m were about 20,000 km^2 when the first sprite

was observed. Soula et al. (2015) also reported that the area of the stratiform region with radar reflectivity greater than 10 dBZ (0.15 mm/h) is about 20000 km^2 at an altitude of 3 km when the first sprite occurred. Sprites tend to occur once an MCS develops considerable stratiform precipitation regions, meaning that the 10 dBZ (0.15 mm/h) region grows larger than 15000–20000 km^2. The period of sprite activity commenced as the radar echo area reached 34000 km^2 (Lyons et al., 2003). In addition, Lyons et al. (2003) indicate that the stratiform precipitation region increases abruptly before sprite emissions begin. Total precipitation areas reached 60000 km^2 and 40000 km^2 when our first and last sprites occurred, although these were not local or maximum peaks. The orders of precipitation areas are the same as in previous papers.

After the convective and stratiform regions of the parent thunderstorm system for the first five sprites were in decay and convective 3 had dissipated, a different convective line (convective 4) developed and matured (the amount of precipitation increased), and precipitation in the stratiform region became weaker than in the previous period (Figure 3g). The sixth sprite with one element was produced by +CG in the convective region (Figure 3h). The azimuth of the sprite element was displaced to the west from the +CG. The intense precipitation area in the convective region became weaker than in the previous period and the area and quantity of precipitation in the stratiform region became smaller. The total precipitation area surpassed 40000 km^2 when the sixth sprite occurred. It was found that all sprites shown in this paper were produced by large thunderstorm systems such as MCSs. As sprite-producing +CGs were located in the convective region, the distribution of cells and charging mechanisms in the convective region seem to play important roles for sprite producing +CG in this case.

As seen in Figures 3f and h, it was found that sprites 1–5 and 6 were produced by +CGs in the stratiform and convective regions, respectively. Strong precipitation rates increased over a period of 80 minutes before the first sprite, while increasing over 30 minutes before the sixth sprite (Figure 2d). This temporal difference in the strong precipitation rate may result from the difference in the principal charging mechanisms in the stratiform and convective regions.

Generally, charging mechanisms in the stratiform region are considered to result from (i) advection into the stratiform region from the convective region and (ii) local (*in situ*) generation of charge in the stratiform region (MacGorman & Rust, 1998). Actually, a case supporting (i) was observed in a leading-line, trailing-stratiform MCS (e.g. Carey et al., 2005). A case supporting (ii) described four charge layers located in the MCS stratiform region (e.g. Stolzenburg et al., 1998). Advection (i) contributes charge to the stratiform region within 60 km of the convective region and local generation (ii) in the stratiform region dominates at distances greater than 60 km (MacGorman & Rust, 1998).

Williams (2017) described that Azambuja (2013) found a time delay of 80–90 minutes between the most lightning-active phase and the time at which sprites initiated by energetic positive ground flashes were prevalent. The time delay is consistent with the descent of ice crystals from the upper troposphere to the

lower portion of the stratiform region.

The first five sprite-producing +CGs described in this study occurred in the western part of the intense precipitation area in the stratiform region. The intense precipitation in the stratiform region (see "stratiform" in Figure 3f), which surpasses the convective region (see convective 3 in Figure 3f), occurred more than 100 km from the eastern edge of the convective region (convective 3). The period of intense precipitation (primarily occurring under the stratiform region) from beginning to peak lasted at least 80 minutes. This is consistent with the time delay found by Azambuja (2013), as mentioned. These facts imply that the primary charging mechanism is the local generation of charge in the stratiform region. Although sprite-producing +CGs can occur due to large charges that accumulate in the stratiform region, we cannot explain why lightning was inactive in the stratiform region nor what triggered the sprite-producing +CGs.

To the contrary, it has been reported that +CGs in the MCS convective region can also occur but are always scarce (Total +CGs were at most 6%) (Holl et al., 1994). In some cases, a large density of positive ground flashes occurs in the convective region (MacGorman & Morgenstern, 1998). Petersen and Rutledge (1992) also reported that the average peak currents of positive ground flashes were 89 kA and 55 kA in the stratiform regions versus 54 kA and 37 kA in the convective regions during two different storm experiment cases. McCormick (2003) stated that the average peak positive current in the stratiform region (43.0 kA) is over two times larger than the average peak positive current in the convective region (20.2 kA). There are many reports that the percentage or number of +CGs in the MCS stratiform region exceeded those in the MCS convective region (e.g. Holle et al., 1994; MacGorman & Morgenstern 1998; Petersen & Rutledge 1992; Rutledge et al., 1990; Rutledge & MacGorman, 1988; Shafer et al., 2000). Therefore, our sixth sprite-producing +CG (89kA: it was the minimum value in our casess) that occurred in the MCS convective region represents a very rare case. Large positive charging mechanisms in the MCS convective region, such as those associated with sprite-producing +CGs, are not well understood.

As in previous studies, very few +CGs were in the convective region with the sixth sprite. Fortunately, we could detect the sixth sprite and the +CG that produced it simultaneously within the same video frames. From the video in Figure 1c, the optical flash in the cloud appeared to propagate from the +CG point located in the eastern part of cloud flash to the west side (the same as the sprite azimuth and +CG point). This may mean that the +CG occurred in a (probably older) convective cell in the eastern part, and its lightning channel extended to different (likely younger) cells in the western part. As for the reason a +CG with sprite occurred in the MCS convective region, we speculate that the sixth sprite-parent +CG removed a large amount of positive charge by gathering positive charges from different convective cells contained in the MCS convective region.

As for positive charge locations in the stratiform region, there are many papers discussing a positive charge layer near the freezing level in the lower part of MCS stratiforms (such as Shepherd et al., 1996). For example, Williams (1999) presented a sprite-causative positive charge reservoir in the lower part of an MCS stratiform. Unfortunately, the extent of the optical flash cannot be found in any of the five sprite images in Figure 1b. The reason is that the MCS stratiform region associated with those five sprites was located more than 300 km from the observatory. If an amount of positive charge large enough to cause a sprite had resided in the lower part of the stratiform MCSs, as suggested by many papers, optical flashes could not have been detected because of mountains and cloud conditions (obstacle optical flash) between the observer and MCS stratiform region, and the effect of Earth's curvature.

4 Conclusions

Fortunately, in these cases, we could separate the time sequences of strong precipitation associated with the first five sprites and the sixth sprite. The reason, as shown in Figures 2 and 3, is that there is a time lag between the peaks of strong precipitation in the stratiform region and the first five sprites and that in the convective region and the sixth sprite. Conclusions for the relationship between the sprites and precipitation in the MCS on 22 July 2013 are as follows:

1. Five sprite-producing +CGs occurred in the MCS stratiform region, and a sixth sprite-producing +CG occurred in the MCS convective region.
2. Sprites occurred close to the local peak time of strong precipitation as compared to total precipitation.
3. The time periods between the beginnings of the precipitation rate increase and the peaks associated with the first or the last sprites are at least 80 minutes for the MCS stratiform region and at most 30 minutes for the MCS convective region.
4. As discussed, it is speculated that the result for the MCS stratiform region means that positive charge is generated locally (*in situ*). In the MCS convective region, positive charge might be gathered and be removed from several neighboring convective cells just before the sprite occurred.

Acknowledgments

This work was performed during the period when the facilities were maintained by the NPO Valid Utilization of Mt. Fuji Weather Station. This research was supported in part by JSPS KAKENHI, 20H02419, 2020-2022 (MK), JSPS KAKENHI, 15K12372, 2015-2017 (MK), Hoso Bunka Foundation GRANTS, 2014 (MK). We thank Yuko Suzuki of Tokyo Gakugei University for observation at Mt. Fuji and Kenichi Kusunoki of the Meteorological Research Institute for much cooperation and support. The data examined were provided by Japan Meteorological Agency. The data are available at http://database.rish.kyoto-u.ac.jp/index-e.html and at cost from http://www.jmbsc.or.jp/en/index-e.html.

References

Adachi, T., Fukunishi, H., Takahashi, Y., Sato, M., Ohkubo, A., & Yamamoto, K. (2005). Characteristics of thunderstorm systems producing winter sprites in Japan. *Journal of Geophysical Research,* 110(D11), D11203. https://doi.org/10.1029/2004JD005012

Azambuja, R. (2013), Thunderstorms producing sprites in South America, (Doctoral dissertation). Sao Jose dos Campos: Instituto Nacional de Pesquisas Espaciais.

Carey, L. D., Murphy, M. J., McCormick, T. L., & Demetriades, N. W. S. (2005). Lightning location relative to storm structure in a leading-line, trailing-stratiform mesoscale convective system. *Journal of Geophysical Research*, 110(D3), D03105. https://doi.org/10.1029/2003JD004371

Franz, R.C., Nemzek, R.J., & Winckler, J.R. (1990). Television image of a large upward electrical discharge above a thunderstorm system. *Science*, 249(4964), 48-51. https://doi.org/10.1126/science.249.4964.48

Fukunishi, H., Takahashi, Y., Uchida, A., Sera, M., Adachi, K., & Miyasato, R. (1999). Occurrence of sprites and elves above the Sea of Japan near Hokuriku in winter. *Eos Transaction AGU*, 80(46), Fall Meeting Supplement F217.

Ganot, M., Yair, Y., Price, C., Ziv, B., Sherez, Y., Greenberg, E., Devir, A., & Yaniv, R. (2007). First detection of transient luminous events associated with winter thunderstorms in the eastern Mediterranean. *Geophysical Research Letters*, 34(12), L12801. http://doi.org/10.1029/2007GL029258

Hayakawa, M., Nakamura, T., Hobara, Y., & Williams, E. (2004). Observation of sprites over the Sea of Japan and conditions for lightning-induced sprites in winter. *Journal of Geophysical Research*, 109(A1), A01312. https://doi.org/10.1029/2003JA009905

Holle, R. L., Watson, A. I., López, R. E., Macgorman, D. R., Ortiz, R., & Otto, W. D. (1994). The Life Cycle of Lightning and Severe Weather in a 3–4 June 1985 PRE-STORM Mesoscale Convective System. *Monthly Weather Review*, 122(8), 1798-1808. https://doi.org/10.1175/1520-0493(1994)122%3C1798:TLCOLA%3E2.0.CO;2

Houze, R. A., Jr. (1977). Structure and Dynamics of a Tropical Squall-Line System. *Monthly Weather Review*, 105(12), 1540-1567. https://doi.org/10.1175/1520-0493(1977)105%3C1540:SADOAT%3E2.0.CO;2

Ishii, K. Syugo H., & Fujibe, F. (2014). Statistical Analysis of Temporal and Spatial Distributions of Cloud-to-Ground Lightning in Japan from 2002 to 2008. *Journal of Atmospheric Electricity*, 34(2), 79-86. https://doi.org/10.1541/jae.34.79

Lang, T. J., Lyons, W. A., Rutledge, S. A., Meyer, J. D., MacGorman, D. R., & Cummer, S. A. (2010). Transient luminous events above two mesoscale

convective systems: Storm structure and evolution. *Journal of Geophysical Research*, 115(A5), A00E22. https://doi.org/10.1029/2009JA014500

Li, J., Cummer, S. A., Lyons, W. A., & Nelson, T. E. (2008). Coordinated analysis of delayed sprites with high-speed images and remote electromagnetic fields. J*ournal of Geophysical Research*, 113(D20), D20206. https://doi.org/10.1029/2008JD010008

Lu, G., Cummer, S A., Li, J., Zigoneanu, L., Lyons, W. A., Stanley, M. A., Rison, W., Krehbiel, P. R., Edens, H. E., Thomas, R. J., Beasley, W. H., Weiss, S. A., Blakeslee, R. J., Bruning, E. C., MacGorman, D. R., Meyer, T. C., Palivec, K., Ashcraft, T., & Samaras, T. (2013). Coordinated observations of sprites and in-cloud lightning flash structure. *Journal of Geophysical Research*, 118(12), 6607-6632. https://doi.org/10.1002/jgrd.50459

Lyons, W.A. (1996). Sprite observations above the U.S. High Plains in relation to their parent thunderstorm systems. *Journal of Geophysical Research*, 101(D23), 29641-29652. https://doi.org/10.1029/96JD01866

Lyons, W. A., Nelson, T. E., Williams, E. R., Cummer, S. A., & Stanley, M. A. (2003). Characteristics of Sprite-Producing Positive Cloud-to-Ground Lightning during the 19 July 2000 STEPS Mesoscale Convective Systems. *Monthly Weather Review*, *131*(10), 2417-2427. https://doi.org/10.1175/1520-0493(2003)131%3C2417:COSPCL%3E2.0.C

MacGorman, D. R., & Rust, W. D. (1998), The electrical nature of storms (pp. 281-282). Oxford, NY, Oxford University Press.

MacGorman, D. R., & Morgenstern, C. D. (1998), Some characteristics of cloud-to-ground lightning in mesoscale convective systems. *Journal of Geophysical Research*, 103(D12), 14011-14023. https://doi.org/10.1029/97JD03221

McCormick, T. L. (2003). Three-dimensional radar and total lightning characteristics of mesoscale convective systems, (master's thesis). Retrieved from North Carolina State University libraries. (https://repository.lib.ncsu.edu/handle/1840.16/1184). NC: North Carolina State University.

Neubert, T., Allin, T.H., Stenbaek-Nielsen, H. & Blanc, E. (2001). Sprites over Europe. *Geophysical Research Letters*, 28(18), 3585-3588. https://doi.org/10.1029/2001GL013427

Neubert T., Allin, T. H., Blanc, E., Farges, T., Haldoupis, C., Mika, A., Soula, S., Knutsson, L., van der Velde, O., Marshall, R. A., Inan, U., Sátori, G., Bór, J., Hughes, A., Collier, A., Laursen, S., & Rasmussen, I. L. (2005). Coordinated observations of transient luminous events during the EuroSprite2003 campaign. *Journal of Atmospheric and Solar-Terrestrial Physics*, 67(8-9), 807-820. https://doi.org/10.1016/j.jastp.2005.02.004

Petersen, W. A., & Rutledge, S. A. (1992). Some characteristics of cloud-to-ground lightning in tropical northern Australia. *Journal of Geophysical Research*, 97(D11), 11553-11560. https://doi.org/10.1029/92JD00798

Pinto, O., Saba, M. M. F., Pinto, I. R. C. A., Tavares, F. S. S., Naccarato, K. P., Solorzano, N. N., Taylor, M. J., Pautet, P. D., & Holzworth, R. H. (2004). Thunderstorm and lightning characteristics associated with sprites in Brazil. *Geophysical Research Letters*, 31(13), L13103. https://doi.org/10.1029/2004GL020264

Rutledge, S. A., & MacGorman, D. R. (1988). Cloud-to-Ground Lightning Activity in the 10-11 June 1985 Mesoscale Convective System Observed during the Oklahoma-Kansas PRE-STORM Project. *Monthly Weather Review*, 116(7), 1393-1408. https://doi.org/10.1175/1520-0493(1988)116%3C1393:CTGLAI%3E2.0.CO;2

Rutledge, S. A., Lu, C., & MacGorman, D. R. (1990). Positive Cloud-to-Ground Lightning in Mesoscale Convective Systems. *Journal of Atmospheric Sciences*, 47(17), 2085-2100. https://doi.org/10.1175/1520-0469(1990)047%3C2085:PCTGLI%3E2.0.CO;2

São Sabbas, F.T., Sentman, D.D., Wescott, E.M., Pinto, O., Mendes, O. & Taylor, M.J. (2003). Statistical analysis of space-time relationships between sprites and lightning, *Journal of Atmospheric and Solar-Terrestrial Physics*, 65(5), 525-535. https://doi.org/10.1016/S1364-6826(02)00326-7

Sentman, D. D., & Wescott, E. M. (1996). Red sprites and blue jets: High-altitude optical emissions linked to lightning, *Eos Transaction AGU*, 77(1), 1- 5. https://doi.org/10.1029/95EO00001

Shafer, M. A., MacGorman, D. R., & Carr, F. H. (2000). Cloud-to-Ground Lightning throughout the Lifetime of a Severe Storm System in Oklahoma. *Monthly Weather Review*, 128(6), 1798-1816. https://doi.org/10.1175/1520-0493(2000)128%3C1798:CTGLTT%3E2.0.CO;2

Shepherd, T. R., Rust, W. D., & Marshall, T. C. (1996). Electric Fields and Charges near 0°C in Stratiform Clouds. *Monthly Weather Review*, *124*(5), 919-938. https://doi.org/10.1175/1520-0493(1996)124%3C0919:EFACNI%3E2.0.CO;2

Soula, S., van der Velde, O., Palmiéri, J., Chanrion, O., Neubert, T., Montanyà, J., Gangneron, F., Meyerfeld, Y., Lefeuvre, F., & Lointier, G. (2010). Characteristics and conditions of production of transient luminous events observed over a maritime storm. *Journal of Geophysical Research*, 115(D16), D16118. https://doi.org/10.1029/2009JD012066

Soula, S., Iacovella, F., van der Velde, O., Montanyà, J., Füllekrug, M., Farges, T., Bór, J., Georgis, J.-F., NaitAmor, S., & Martin, J.-M. (2014). Multi-instrumental analysis of large sprite events and their producing storm in southern France. *Atmospheric Research*, 135-136, 415-431, https://doi.org/10.1016/j.atmosres.2012.10.004

Soula, S., Defer, E., Füllekrug, M., van der Velde, O., Montanya, J., Bousquet, O., Mlynarczyk, J., Coquillat, S., Pinty, J.-P., Rison, W., Krehbiel, P.R., Thomas, R., & Pedeboy, S. (2015). Time and space correlation between sprites and their parent lightning flashes for a thunderstorm observed during the

HyMeX campaign. *Journal of Geophysical Research*, 120(22), 11552-11574. https://doi.org/10.1002/2015JD023894

Stolzenburg, M., Rust, W. D., Smull, B. F., & Marshall, T. C. (1998). Electrical structure in thunderstorm convective regions: 1. Mesoscale convective systems. *Journal of Geophysical Research*, 103(D12), 14059-14078. https://doi.org/10.1029/97JD03546

Su, H.-T., Hsu, R.-R., Chen, A. B. -C., Lee, Y. -J., & Lee, L.-C. (2002). Observation of sprites over the Asian continent and over oceans around Taiwan. *Geophysical. Research Letters*, 29(4), 1044, 3-1-3-4. https://doi.org/10.1029/2001GL013737

Suzuki, T., Hayakawa, M., Matsudo, Y., & Michimoto, K. (2006). How do winter thundercloud systems generate sprite-inducing lightning in the Hokuriku area of Japan? *Geophysical Research Letters*, 33(10), L10806. https://doi.org/10.1029/2005GL025433

Suzuki, T., Hayakawa, M., Hobara, Y., & Kusunoki, K. (2012). First detection of summer blue jets and starters over Northern Kanto area of Japan: Lightning activity. *Journal of Geophysical Research*, 117(A7), A07307. https://doi.org/10.1029/2011JA017366

Takahashi, Y., Miyasato, R., Adachi, T., Adachi, K., Sera, M., Uchida, A., & Fukunishi, H. (2003). Activities of sprites and elves in the winter season, Japan. *Journal of Atmospheric and Solar-Terrestrial Physics*, 65(5), 551-560. https://doi.org/10.1016/S1364-6826(02)00330-9

van der Velde, O. A., Mika, Á., Soula, S., Haldoupis, C., Neubert, T., & Inan, U. S. (2006). Observations of the relationship between sprite morphology and incloud lightning processes. *Journal of Geophysical Research*, 111(D15), D15203. https://doi.org/10.1029/2005JD006879

van der Velde, O.A., Montanyà, J., Soula, S., Pineda, N., & Bech, J., (2010). Spatial and temporal evolution of horizontally extensive lightning discharges associated with sprite-producing positive cloud-to-ground flashes in northeastern Spain. *Journal of Geophysical Research*, 115(A9), A00E56. http://dx.doi.org/10.1029/2009JA014773

Williams, E. R. (1998). The positive charge reservoir for sprite-producing lightning. *Journal of Atmospheric and Solar-Terrestrial Physics*, 60(7-9), 689-692. https://doi.org/10.1016/S1364-6826(98)00030-3

Williams, E.R., Lyons, W.A., Hobara, Y., Mushtak, V.C., Asencio, N., Boldi, R., Bór, J., Cummer, S.A., Greenberg, E., Hayakawa, M., Holzworth, R.H., Kotroni, V., Li, J., Morales, C., Nelson, T.E., Price, C., Russell, B., Sato, M., Sátori, G., Shirahata, K., Takahashi, Y., & Yamashita, K. (2010). Ground-based detection of sprites and their parent lightning flashes over Africa during the 2006 AMMA campaign. *Quarterly Journal of the Royal Meteorological Society*, 136(S1), 257-271. https://doi.org/10.1002/qj.489

Williams, E. (2018). Lightning Activity in Winter Storms: A Meteorological and Cloud Microphysical Perspective. *IEEJ Transactions on Power and Energy*, 138(5), 364-373. https://doi.org/10.1541/ieejpes.138.364